Biosensors and Bioelectronics 67 (2015) 100–106

Contents lists available at ScienceDirect

Biosensors and Bioelectronics

journal homepage: www.elsevier.com/locate/bios

Whole-cell based label-free capacitive biosensor for rapid nanosize-dependent toxicity detection

Anjum Qureshi [a,*], Ashish Pandey [a,b], Raghuraj S. Chouhan [a], Yasar Gurbuz [b], Javed H. Niazi [a,**]

[a] Sabanci University Nanotechnology Research and Application Center, Orta Mah., 34956 Istanbul, Turkey
[b] Faculty of Engineering and Natural Sciences, Sabanci University Orhanli, 34956 Istanbul, Turkey

ARTICLE INFO

Article history:
Received 4 June 2014
Received in revised form
16 July 2014
Accepted 17 July 2014
Available online 23 July 2014

Keywords:
Fe_3O_4 nanoparticles
Nanotoxicity
E. coli
Whole-cell biosensor
Capacitive biosensor

ABSTRACT

Despite intensive studies on examining the toxicity of nanomaterials (NMs), our current understanding on potential toxicity in relation to size and cellular responses has remained limited. In this work, we have developed a whole-cell based capacitive biosensor (WCB) to determine the biological toxicity of nanoparticles (NPs) using iron oxide (Fe_3O_4) NPs as models. This WCB chip comprised of an array of capacitor sensors made of gold interdigitated microelectrodes on which living *Escherichia coli* cells were immobilized. Cells-on-chip was then allowed to interact with different sizes of Fe_3O_4 NPs (5, 20 and 100 nm) and concentration-depended cellular-responses were measured in terms of change in dielectric properties (capacitance) as a function of applied AC frequency. The WCB response showed smaller-sized Fe_3O_4 NPs (5 nm) induced maximum change in surface capacitance because of their effective cellular interaction with *E. coli* cells-on-chip indicating that the cells suffered from severe cellular deformation, which was confirmed by scanning electron microscopic (SEM) examination. Further our results were validated through their cell viability and *E. coli* responses at the interface of cell-membrane and NPs as a proof-of-concept. WCB response showed a size-dependent shift in maximum response level from 2 μg/ml of 5 nm sized NPs to 4 μg/ml with NP-sizes greater than 20 nm. The developed WCB offered real-time, label-free and noninvasive detection of cellular responses against Fe_3O_4 NPs' toxicity with speed, simplicity and sensitivity that can be extended to toxicity screening of various other NPs.

1. Introduction

The nanotechnology industry is rapidly growing with promises of substantial benefits that will have significant economic and scientific impacts. Use of nanomaterials including metal and metal oxide nanoparticles, nanotubes, nanowires and quantum dots are applicable to a whole host of areas ranging from aerospace engineering and nano-electronics to environmental remediation and medical healthcare (Nel et al., 2006; Seetharam and Sridhar, 2007). However, with this rapid development, these nanomaterials (NMs) potentially carry unintended hazards. Expanding use of NMs and commercialization of NM-related products bound to increase the standardization of methods in testing of their potential toxicity to the environment and human. Currently, a complete understanding of the size, shape, composition and aggregation-dependent interactions of nanostructures with biological systems is lacking. It is primarily due to the choices of the many possible parameters including variability of methods, materials used and cell-types employed for testing toxicities (Pompa et al., 2011).

Physiochemical interactions between engineered NPs and cell-surfaces play a crucial role in their toxicities (Nel et al., 2006, 2009; Zhang et al., 2012). The interaction of NPs with cell-surface functional groups such as trans-membrane protein may cause reversible and irreversible changes in the physiochemical properties of cells, which result in partial or complete structural damage (Nel et al., 2009). Recently, engineered NPs interaction with bacterial cells is reported to occur through disorganization, permeability changes and deformation in the bacterial cell membrane (Morones et al., 2005; Zhang et al., 2012). For example, biomechanical studies with hematite NPs showed deformation in *E. coli* cells through possible disruption of surface appendages (Zhang et al., 2012). Other studies showed the Ag NPs adhering to the *E. coli* cell-surface and thus altering the membrane properties and affecting the cellular permeability and respiration (Morones et al., 2005). To date, most traditional biological methods for *in vitro* and *in vivo* toxicological studies of engineered NMs on microbial cells are based on cellular activity and proliferations.

* Corresponding author. Tel.: +90 216 483 9000x2441.
** Corresponding author. Tel.: +90 216 483 9879; fax: +90 216 483 9885.
E-mail addresses: anjum@sabaniuniv.edu (A. Qureshi), javed@sabanciuniv.edu (J.H. Niazi).

http://dx.doi.org/10.1016/j.bios.2014.07.038
0956-5663/

These methods include growth and viability assays (Chatterjee et al., 2011; Oberdorster et al., 2005), proteomic assays, reactive oxygen species (ROS) detection tests (Brunet et al., 2009; Choi and Hu, 2008), and molecular-level evaluations based on genetic responses (Mcquillan and Shaw, 2014; Xie et al., 2011). Among all the above methods, *in vitro* cytotoxicity methods are currently employed, which required labeling with fluorescent molecules for detection. These methods are used as markers for cell-viability and consist of procedures that provide results only at a final time-point (Hussain et al., 2005). The existing methods reported in the literature are expensive that require chemical reagents or chromogenic mediators and complicated operation to generate the detectable signal and often leading to undesirable quenching effects with NPs.

Investigating the impacts of interactions between NPs and cell-surfaces through electrical and physical properties are important for interpreting toxicity data, and predicting the toxicity risks associated with engineered NPs. Interdigitated gold microelectrode based impedimetric sensors offer easy-to-use and miniaturized device for measuring trace amounts of toxic compounds (Ribeiro et al., 2010). Such sensors can be interfaced with whole-cells as biological transducers for biosensor applications. Whole-cell biosensors offer an alternative approach to existing methods for detecting nanotoxicities, because they are able to provide information about noninvasive total physiological effect of a nano-sized material toward a living-cell. In this study, we designed a WCB chip, which is capable of noninvasively sensing the size and concentration dependent toxic effects using model Fe_3O_4 NPs. This WCB measures the capacitance from immobilized cells over electrodes as a function of applied AC frequency. Changes in capacitance can be detected that occurred as a result of changes in the cellular activity after their interaction with NPs. The WCB chip offers compact structure, ease of use and the ability to measure multiple samples and monitoring capabilities for cytotoxicity determination. The results obtained from the WCB studies were confirmed through surface morphological changes with scanning electron microscopic (SEM) examinations as well as probing cellular interactions at the cell-membrane and NPs interfaces.

2. Experimental

2.1. Chemical and reagents

Silicon wafers of 4 in. size, ⟨100⟩ oriented, p-type with the resistivity of 9–12 Ω cm and thicknesses of 500 ± 25 μm with 1 μm thick SiO_2 layer on top were obtained from University Wafers, USA. Wild-type *E. coli* DH5α strain was used as model living bacterial cells in this study. Luria-Bertani broth (LB-broth) and Luria-Bertani agar (LB-agar) were obtained from Difco (MI, USA). Phosphate-buffered saline (PBS), 3-mercaptopropionic acid (MPA), 1-Ethyl-3-[3-dimethylaminopropyl] carbodiimide hydrochloride (EDC) and *N*-hydroxysuccinimide (NHS), Fe_3O_4 nanoparticles (with sizes of 5, 20 and 100 nm) were purchased from Sigma-Aldrich, Germany and Qdot® 625 ITK™ carboxyl quantum dots were purchased from Life Technologies (Invitrogen).

2.2. Fabrication of capacitor array chip

Gold interdigitated microelectrode array based capacitors were patterned on a 525 ± 25 μm thick SiO_2 wafers (p-type, 0–100 Ω cm resistivity, ⟨100⟩ orientation) using standard photolithography. The wafer surface was cleaned in a series of steps using isopropanol, acetone and distilled water, respectively and dried using N_2 gas. Image reversal was carried out using AZ5214E photoresist after layering it on SiO_2 wafers and baked at 120 °C for 5 min. Following this step, a 50–60 nm thin titanium layer was deposited to facilitate improved adhesion of gold and a 200–210 nm thick gold layer was then deposited using direct current sputter deposition. The deposition was carried out in argon atmosphere with power of 150 W for 3 min. The gold was lifted off using acetone and the dimension of each electrode was measured to be 800 μm in length and 40 μm in width with a distance between two electrodes of 25 μm. Each wafer contained 45 independent capacitors in arrays each made of 24 gold microelectrodes within a total area of 3 mm^2 that served as individual sensors. The characterization of gold microelectrode surface of capacitor was performed by Atomic Force Microscopy (AFM, Nanoscope) with the tapping mode.

2.3. E. coli culture preparation

Actively growing *E. coli* cells were inoculated into a fresh LB-medium and grown till reaching to a mid-logarithmic growth phase. Cells were then harvested by centrifugation at 1000*g* for 3 min and washed the cell-pellet thrice by resuspending in PBS buffer, pH 7.2 and finally resuspended in the same buffer. The cell concentration was determined by measuring OD_{600} and alternatively by colony counting after serial dilution followed by plating on LB-agar plates.

2.4. Surface chemistry and immobilization of cells

Capacitor array chip was subjected to plasma cleaning followed by washing thoroughly with ethanol and finally dried using N_2 gas. Self-assembled monolayer (SAM) was formed using MPA on gold microelectrodes of capacitor array chip. For this, the chip was immersed in 20 mM of ethanolic MPA and incubated overnight at room temperature. After the SAM formation, the chip was washed thrice with water and dried using N_2. The chips were then incubated with a mixture of 100 mM EDC and 50 mM of NHS for 2 h and thoroughly washed with distilled water. The surface-activated capacitor chips were incubated with three different concentrations of bacterial cell suspensions (8×10^5, 8×10^6 and 8×10^7 cells) in 5 μl PBS solution for 2 h. The cell-numbers on sensors was optimized by their capacitive performances and the optimized colony forming units (cfu) on sensor surface area of 3 mm^2 was determined. The immobilized cell numbers (cfu) that exhibited significant change in dielectric properties (impedance/capacitance) was found to be 8×10^7 cfu under normal conditions, which was subsequently maintained on all capacitor array chips for further studies. The surface of chip immobilized with different concentration of *E. coli* cells were also examined using an optical microscope (Carl Zeiss Axio Scope) at different magnifications to observe the uniformity of cell-layers on microelectrodes.

2.5. Exposure of different sizes and concentrations of Fe_3O_4 NPs on WCB chip

Fe_3O_4 NPs of sizes 5 and 20 nm were commercially available in the form of homogeneous suspension in toluene as a solvent, while the larger sized NPs (100 nm) were readily available suspended in water. Therefore, Fe_3O_4 NPs were first diluted in PBS (pH 7.4) containing 5% ethanol mixture. The trace levels of toluene carried after the dilution along with 5% ethanol from the final suspension was rapidly evaporated by purging with N_2 gas before incubating the sample on WCB chip, and therefore the probable effects derived from toluene/ethanol were prevented from interfering in chip responses. A similar process was repeated for control samples except with no NPs. The diluted Fe_3O_4 NPs suspensions were prepared just before to their incubation on the WCB chips to prevent from agglomeration. In this way, three different sizes of

iron oxide (Fe_3O_4) NPs with 5, 20 and 100 nm at different concentrations (0.2, 0.4, 0.6, 2, 4, 8 μg/ml), respectively were incubated on WCB chips. The area of each capacitor in WCB chip was made of 24 gold interdigitated microelectrodes in an array, immobilized with *E. coli* cells measuring 3 mm^2 sensing area. This sensing area was incubated for 1 h at 25 °C with 5 μl volumes of Fe_3O_4 NPs of the different size and concentrations indicated above. After the incubation, the WCB chip was quickly washed with PBS solution and dried using a N_2 gun before taking dielectric measurements.

2.6. Dielectric measurements (impedance/capacitance)

The impedance/capacitance responses were measured before and after the exposure of NPs on the WCB chip surface by non-Faradaic electrochemical impedance spectroscopy (nFEIS). First, the capacitance/impedance were measured sequentially to ensure chips qualify at the end of every processing steps that included; (a) bare capacitors, (b) capacitors immobilized with cells (WCB), (c) WCB after exposure of different sizes of NPs at different concentrations. The capacitance response in between the gold interdigitated microelectrodes of capacitors was measured in the frequency range 50 MHz to 300 MHz using a Network Analyzer (Karl-Suss PM-5 RF Probe Station and Agilent-8720 ES), which was pre-calibrated using SOLT (short-open-load-through) method. The impedance values were exported to MATLAB® software for the analysis and capacitance values of triplicate experiments were extracted at an effective frequency (f) range between 100–300 MHz and normalized with respect to blank controls. The relative capacitance variations were calculated from the data obtained at 200 MHz frequency under standard assay conditions using the following Eq. (1) as described previously (de Vasconcelos et al., 2009),

$$\frac{C - C_0}{C_0} \times 100 \quad (1)$$

where C is the actual capacitance after the interaction of each sizes of NPs with *E. coli* cells at a particular concentration and C_0 is the capacitance before interaction. For control, *E. coli* immobilized chips were treated with only PBS solution in place of NPs (blank/control). A negative control experiment was conducted using WCB chip containing attenuated or heat-killed *E. coli* cells. For this, chips containing immobilized with same number of *E. coli* cells (8×10^7) were subjected to heat treatment in an air-tight and pre-heated humid chamber at 95 °C for 5 min followed by quickly freezing at −70 °C for 5 min and thawed at 25 °C for 15 min. The above treatment process was repeated thrice and finally the chip was dried using N_2 gas before taking measurements as negative controls. Technical and biological replicates ($n=3$) were determined and the percent relative standard deviations (%RSD) was calculated to be within 11%, and the standard deviations were shown as error bars in figures.

2.7. Contact angle measurements and morphological changes in cells

The contact angles of living and heat-killed-cells-on-chip with solution containing 5 and 100 nm NPs at different concentrations were measured as described Supporting information (SI) section. Morphological changes in *E. coli* cells induced by the Fe_3O_4 NPs (5 and 100 nm, respectively with 2 μg/ml concentration) were examined by using SEM (LEO Supra 35VP).

2.8. Validation of WCB response through fluorescence assay and cell viability tests

Cell viability was confirmed by (a) fluorescence assays and (b) viable cell count (cfu). Fluorescence experiment was conducted by covalently coupling quantum dots (QD) with emission at 625 nm on viable *E. coli* cell-surfaces as a fluorescent marker (*E. coli*-QD bioconjugates) and the methods for preparation of bioconjugates were same as described previously (Chouhan et al., 2014). These bioconjugates were used for fluorescence measurements as relative fluorescence units (RFU) and cell-viability tests were performed by incubating the cells with 2 μg/ml of different sized (5, 20 and 100 nm) Fe_3O_4 NPs for 1 h at 37 °C. About 2 μl of the treated *E. coli*-QD bioconjugates (8×10^7 CFU/ml) were used to measure the fluorescence emissions after a blue LED illumination and observed the changes in characteristic emission (RFU) peak at 625 nm from QDs present on cells using Fluorospectrometer (Nanodrop 3300, Thermo scientific). For cell-viability tests, aliquots of *E. coli*-QD bioconjugates treated with Fe_3O_4 NPs were withdrawn, diluted appropriately and spread onto LB agar plates and incubated overnight at 37 °C. Untreated *E. coli*-QD bioconjugates were used as control and the cfu were counted to compare with control plates and calculated the survival rates using following Eq. (2).

$$\text{Survival rate\%} = \frac{\text{Number of test CFUs}}{\text{Number of control CFUs}} \quad (2)$$

3. Results and discussions

3.1. Sensor surface characterization

Initially, capacitor arrays were fabricated using photolithography technique as described in experimental section. Surface topology of the capacitor chips were examined by AFM images and the topography of gold-interdigitated microelectrodes showed well-distributed and uniformly patterned gold NPs (~100–200 nm sizes) on sensors which was essential for the sensitivity of the sensors through providing large surface area (SI, Fig. S1a and b). AFM 3D height map image showed varying heights of the gold NPs within 2.7 μm^2 scanned area of microelectrode providing sufficient roughness favoring the attachment of cells through first by physical adsorption which is most favorable for efficient chemical coupling (SI, Fig. S1a inset).

3.2. E. coli cell density on capacitor sensor chip

To optimize the bacterial cell-density, varying cell concentrations (10^5–10^7 cfu) were immobilized on capacitor sensor surface. Optical micrographs of capacitor surface immobilized with minimum (8×10^5 cfu) and maximum (8×10^7 cfu) *E. coli* cell densities were examined (Fig. 1a–f). Higher cell density of 8×10^7 cfu resulted in densely packed cells on sensor surface clearly distinguishing from those of lower cell-densities (Fig. 1d–f). The non-specific adsorption on the SiO_2 surface of the chips was observed that evoked with repeated washing of chips with PBS which did not affect the sensor responses.

Capacitance responses with varying densities of *E. coli* cells on WCB chip were measured as a function of scanned AC electrical frequency (50–300 MHz) and the cell density-dependent increase in capacitance responses were recorded (Fig. 2). The dielectric changes occurred with intact bacterial cells was possibly because of their conducting cytoplasmic core, which is contained by a thin insulating membrane surrounded by a porous conducting cell-wall. At low applied AC frequencies (50–200 MHz), capacitance

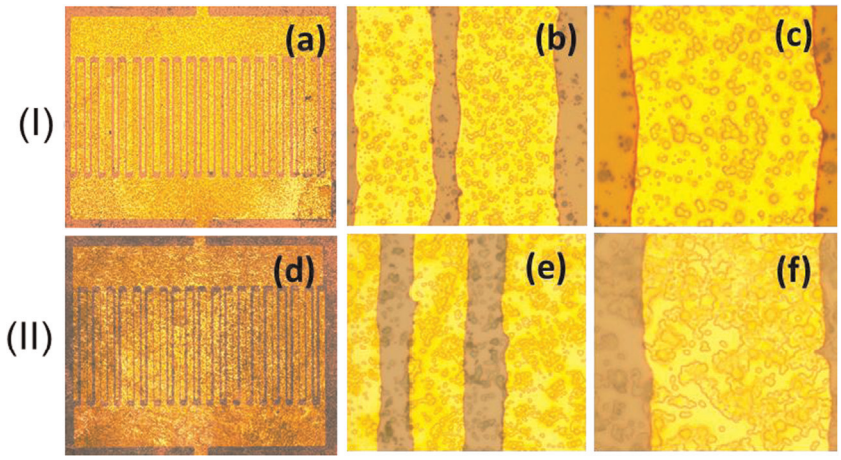

Fig. 1. Optical micrographs of unstained WCB chip surface: MPA-SAM activated chips immobilized with *E. coli* with concentrations of (I) 8×10^5 and (II) 8×10^7 cells. The rows (a–c, and d–f) indicate optical resolutions of $5\times$, $20\times$ and $100\times$, respectively.

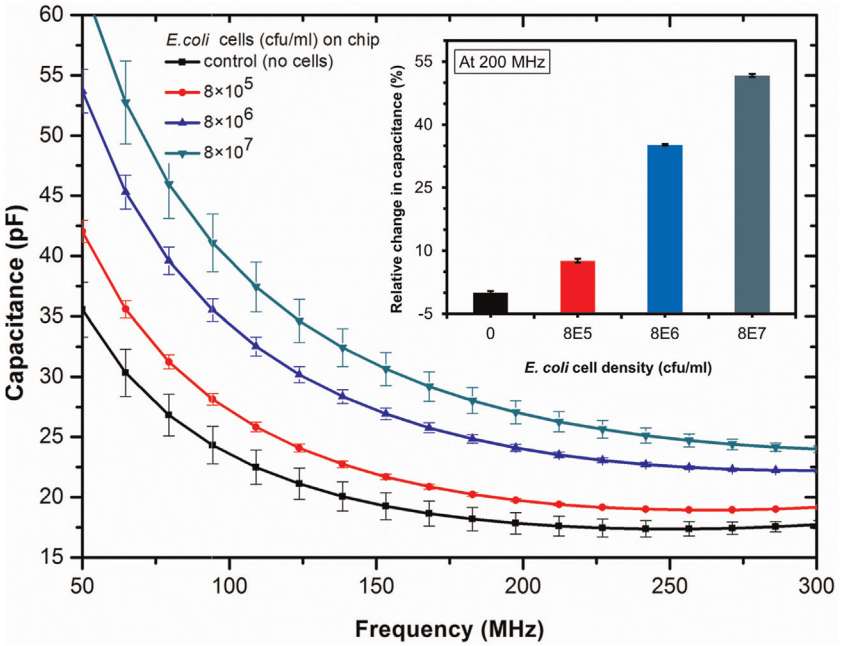

Fig. 2. Capacitive response profile of WCB chips immobilized with three different concentrations of living *E. coli* cells (8×10^5–10^7). The inset figure shows relative change in capacitance of WCB chip response at 200 MHz frequency.

response was more dependent on cell-density while it becomes less dependent on the cells beyond 200 MHz (Fig. 2). Cells exposed to AC electrical frequency field result in an effective movement of layers of ions at both internal and external surfaces of the cell-wall, and becomes electrically polarized (Hodgson and Pethig, 1998). This polarization takes the form of electrical charges that are created on external and interfacial surfaces, which may have influenced the increase in response with cell-density. Lower the applied AC frequency (50–200 MHz), maximum was the interfacial polarization and thus larger the capacitance change (Fig. 2).

Cell-density dependent responses of cells on WCB chip with respect to control (without cells) showed clear distinction in relative change in capacitance as shown in Fig. 2 inset. The cell concentration of 8×10^7 cfu yielded enhanced responses (Fig. 2 inset). Thus, cell-concentration of 8×10^7 cfu was found to be an effective cell-density on 3 mm^2 working area of a capacitor sensor enabling maximum resolution in capacitance responses of the developed WCB chip.

3.3. Biosensing size and concentration of Fe_3O_4 NPs using WCB chip

Capacitive responses of WCB chip before and after the treatment with three different sizes and concentrations were studied. Here, measuring principle for determining toxicity was based on the change in relative surface capacitance induced by the interaction of *E. coli* cells with NPs (with size and/or concentration). The resulting change or re-distribution of surface charges occurred as a result of *E. coli*-NPs complex formation or the collapse of cell-structure on the WCB chip surface as illustrated in Scheme 1.

The ability of WCB chip to respond to NPs was tested by incubating three distinct nano-range sizes (5, 20 and 100 nm) at varying concentrations (0.2–8 μg/ml, 0.9–43 μM) of NPs for 2 h. Control WCB chip was incubated with only PBS solution under identical conditions. The electrical responses of WCB against different sizes and concentrations of NPs were examined using nFEIS against AC electrical frequency sweep from 100 to 300 MHz (Fig. 3a–c). It was observed that the NPs' size dependent responses at different concentrations were dependent on applied frequency

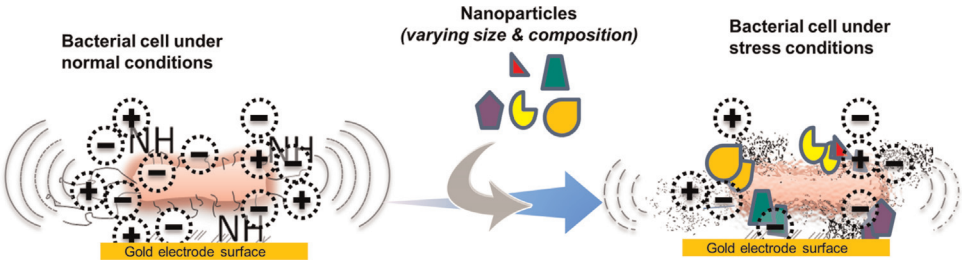

Scheme 1. Schematic illustration of changes in a bacterial cell before and after interaction with Fe_3O_4 NPs on electrode surface of WCB chip.

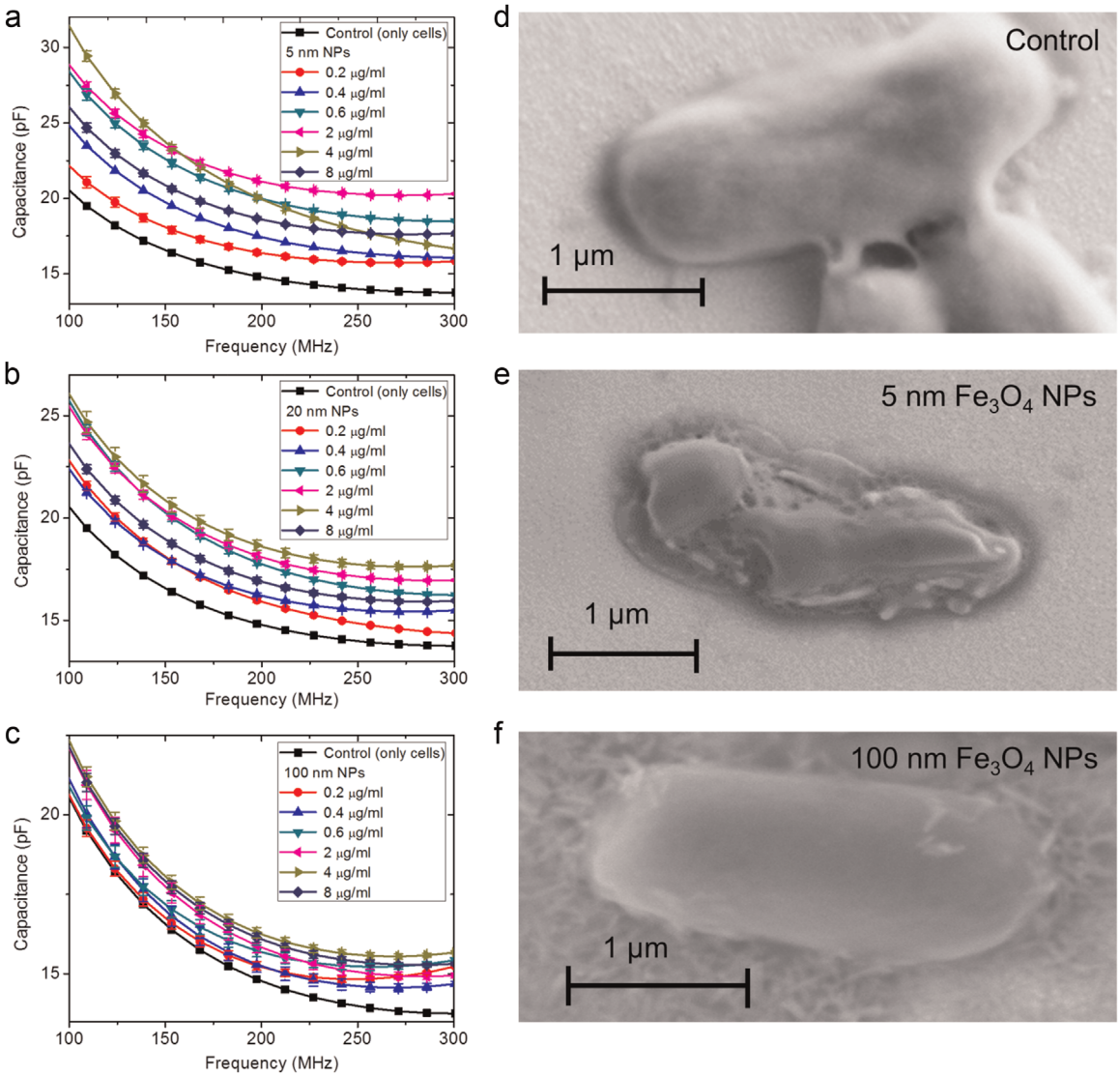

Fig. 3. Changes in capacitance responses using WCB chip against different sizes of Fe_3O_4 NPs such as (a) 5 nm, (b) 20 nm and (c) 100 nm at varying concentrations indicated in the figure legends. On the right panel, SEM images showing (d) healthy/control cells and cells exposed to (e) 5 nm and (f) 100 nm Fe_3O_4 NPs.

(Fig. 3a–c). However, the size dependent capacitive response signal was less dependent on concentration of NPs beyond 250 MHz frequency.

Capacitance response profiles with 5 and 20 nm sized NPs exhibited distinct strengths with respect their responses to different concentrations (Fig. 3a and b). Here, smaller 5 nm sized NPs showed highly dynamic responses with up to a maximum of 2 μg/ml compared with 4 μg/ml with 20 nm NPs, respectively. This shift in threshold concentration levels from 2 to 4 μg/ml was associated with increased size of NPs from 5 to 20 nm, respectively. This result indicated the detrimental effects on cells with smaller sized NPs which can be attributed to cellular damage or disorganization of cell-surface charges. Cellular morphological changes as examined by SEM analysis confirmed the physical damage occurred on cells with 5 nm NPs compared with normal cells (Fig. 3d and e). NPs shown to exhibit high sorption affinity toward *E. coli* due to the attractive interfacial forces as also suggested in the literature reports (Zhang et al., 2012, 2011). A similar effect was also observed with living cells-on-chip against 5 and 100 nm sized Fe_3O_4 NPs that exhibited increased surface hydrophilicity with increasing NPs concentration compared with negative control, heat-killed-cells-on-chip (SI, Table S1). Larger size of 100 nm NPs

were relatively less toxic as evidenced by small changes in capacitance values against different concentrations, as well as with intact cellular morphology (Fig. 3c and f). Capacitance responses of WCB chip with 100 nm NPs followed the same pattern as that of WCB chip responses seen with 20 nm NPs with respect to NPs' threshold concentration, where the maximum response still seen at 4 μg/ml. However, cellular morphology with cells exposed to NPs sizes 20 and 100 nm varied, in which 20 nm NPs induced cellular damage similar to that observed for 5 nm NPs (Fig. 3e). In contrast, 100 nm sized NPs did not reveal any detrimental effect on cells as evidenced from the SEM images obtained from 100 nm NPs treated cells that had intact cellular structure (Fig. 3f). The NPs concentration greater than 4 μg/ml appeared to be lethal to the cells-on-chip, irrespective of their sizes, because the sensor failed to respond to 8 μg/ml NPs of 5–100 nm sizes.

It was possible to monitor the response of WCB chip at a specific frequency as the response was dynamic to the frequency sweep from 100–300 MHz. Therefore, an effective frequency of 200 MHz was selected to extract the sensor signal and normalized capacitance values. This signal enabled elucidating the distinct responses of *E. coli* cells against different nano-sizes and concentrations (Fig. 4 and inset). The heat-killed or dead-cells-on-chip however failed to respond to Fe_3O_4 NPs suggesting that the sensor responses were indeed originated from the living activities of cells-on-chip interacting with NPs (Fig. 4 inset).

The underlying hypothesis of the developed *E. coli* based capacitive biosensor can therefore be explained by following principles. A complex bacterial cell surface consists of positive and negative charges that are constituted from the ionizable side chains of surface and pili-proteins in the outer membrane (Dickson and Koohmaraie, 1989; Magnusson et al., 1980). A typical bacterial cell, behave similar to a globular protein with surface charges that constitute an electric dipole (Qureshi et al., 2010). The simplest molecular dipole in a context of a bacterial cell (*E. coli*) made of a pair of opposite electrical charges with magnitudes of '$+q$' and '$-q$' separated by a vector distance 'r'. The molecular dipole moment 'm' can therefore be given as '$m=qr$'. If a bacterial cell immobilized on a solid surface interacts with NPs, the cells experience a stressful condition due to perturbations on their outer cell membranes which eventually become fragile or disintegrate to exhibit altered surface charge distribution (Narayanan and Chou, 2008).

Interactions of bacterial cells with NPs' above threshold concentrations probably have yielded a reduction in net surface charges, and therefore, a decrease in relative change in capacitance response was evident. This reduction in net charges could be due to the loss of the cells' membrane function imposed by NPs' stress, which resulted in consequent membrane porosity to ions accompanied by extra cytoplasmic protein misfolding (Hodgson and Pethig, 1998; Raffa and Raivio, 2002). Therefore, maximum damage or deformation in cells was likely to occur with concentrations beyond 2 μg/ml of 5 nm and 4 μg/ml for 20–100 nm Fe_3O_4 NPs sizes. This was further confirmed by WCB responses with a negative control experiment in which the *E. coli* cells were attenuated by heat-killing (Fig. 4 inset) demonstrating the specificity of living cellular activity of immobilized *E. coli* on sensor chip.

3.4. Fluorescence assay and cell viability tests for WCB response validation

For the proof-of-concept and validation of WCB responses, fluorescence assay and cell-viability tests were carried out using previously described method involving *E. coli*-QD bioconjugates (Chouhan et al., 2014). The extent of toxicity in *E. coli*-QD bioconjugates treated with three different sized (5, 20 and 100 nm) Fe_3O_4 NPs at 2 μg/ml concentration was measured by the residual fluorescence emission (RFU) and viable cell counts on LB-agar plates. The results showed that the disintegration of fluorescence intensity was dependent on the smaller size which was consistent to the WCB responses, where the order of

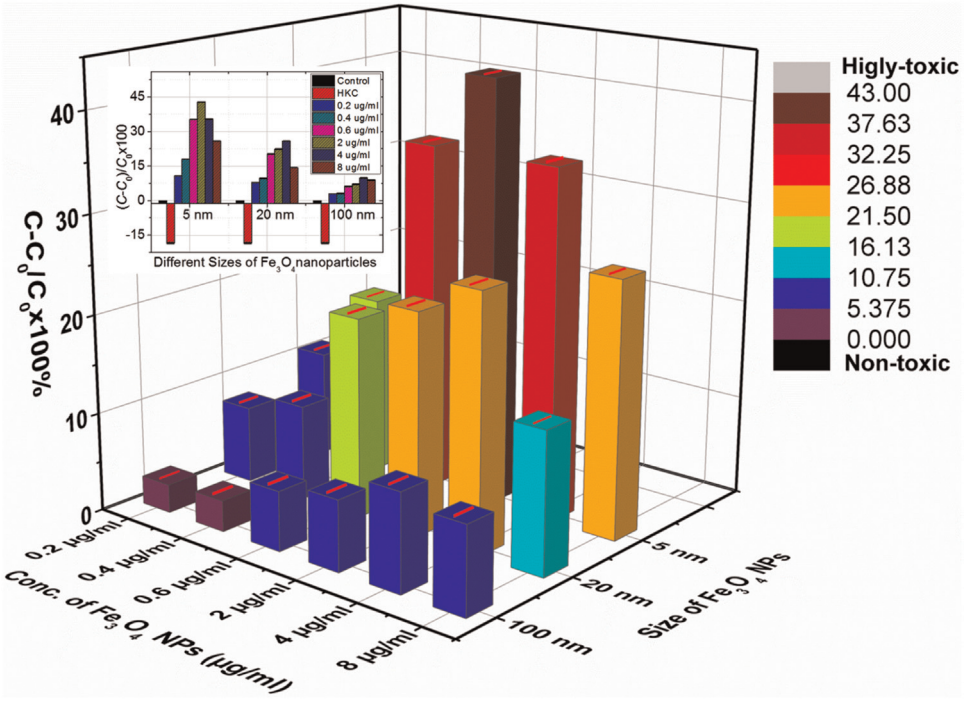

Fig. 4. Relative capacitance responses from WCB chip against varying sizes such as 5, 20 and 100 nm of Fe_3O_4 NPs as a function of applied frequency at 200 MHz. The values in color map scale indicate low to high relative capacitance responses of whole-cell chip designating for non-toxic to highly-toxic nature of NPs. The inset figure shows relative capacitance responses of living and heat-killed cells (HKC) on chip for comparison.

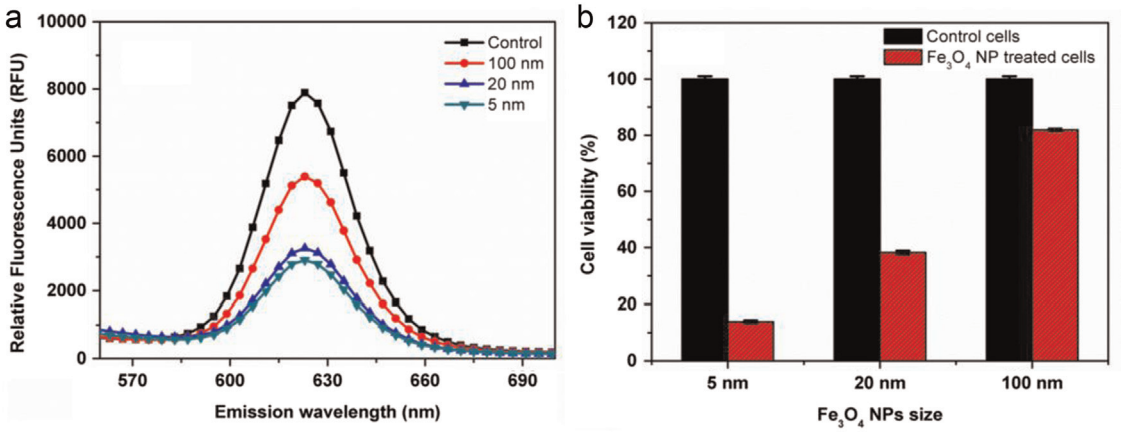

Fig. 5. (a) Residual fluorescence emission profile of *E. coli*-QD bioconjugates and (b) cell viability of *E. coli* cells treated with 5, 20 and 100 nm sizes of Fe_3O_4 nanoparticles at 2 μg/ml concentration.

increasing toxicity followed the order of decreasing NPs size (100 nm < 20 nm < 5 nm) (Fig. 5a). The size dependent toxicity was very well explained as in the case of 100 nm Fe_3O_4 NPs which did not show significant change in fluorescence intensity (Fig. 5a). The above result clearly indicated the direct relationship between fluorescence intensity and toxicity which enabled validating the WCB responses. Further, viability tests with cells treated with NPs also revealed consistent results in which 5 nm and 20 nm NPs imposed 85% and 62% cellular growth reduction, respectively. Larger sized NPs (100 nm) exhibited mild toxic effect with a cell growth reduction of only ~18% (Fig. 5b).

The results obtained from fluorescence assay and cell viability tests were in good accordance with the WCB chip results, provided an effective means for validation. Further, it also inferred that the transduced signal reflected by the WCB on interactions between bacteria and nanomaterials is not just associated with the interplays at nano-bio-interface, but is strongly associated with the toxicity of NPs on the bacterial cells.

4. Conclusions

Assessing the toxicity of NMs for safe handling is imperative for expanded use and commercialization of nanotechnology products. In this work, we have designed and developed a whole-cell based lab-on-chip platform and successfully evaluated its suitability for size-dependent NPs' toxicity determination. The developed WCB chip was tested by label-free and cost-effective method which is based on non-Faradaic electrochemical principles. Our results demonstrated that the WCB chip exhibited size-dependent capacitive responses originating from the interaction of living bacterial cells with different sizes (5, 20 and 100 nm) and concentrations of Fe_3O_4 NPs (0.2–8 μg/ml). The WCB-chip was sensitive and highly specific which was confirmed by employing attenuated cells-on-chip which failed to respond against NPs stresses. The results obtained from fluorescence assay and cell viability tests were in good agreement with the WCB chip results and validated its responses. Further, the WCB results presented in this paper also inferred that the transduced signal on WCB due to interactions between bacteria and NPs was not only associated with the interplays at nano-bio-interface, but is also strongly associated with the toxicity of NPs on the bacterial cells.

WCB chip made of multiple arrays of capacitor sensors enables rapid and real-time screening of samples in multi-sample settings thus creating a versatile, noninvasive tool for sensitive nanotoxicity detection. However, there are a few challenges, such as (a) improving the sensitivity through better design and geometry of electrodes in nano-sizes, (b) integrating microfluidics for small volume sample handling and (c) portability are the current challenges that are aiming to accomplish in this laboratory.

Acknowledgments

This work was supported by the Scientific and Technological Research Council of Turkey (TUBITAK), Project Grant no. 112E051 for AQ. We thank Mehmet Dogan for helping with chip fabrication/processing.

Appendix A. Supplementary information

Supplementary data associated with this article can be found in the online version at http://dx.doi.org/10.1016/j.bios.2014.07.038.

References

Brunet, L., Lyon, D.Y., Hotze, E.M., Alvarez, P.J., Wiesner, M.R., 2009. Environ. Sci. Technol. 43, 4355–4360.
Chatterjee, S., Bandyopadhyay, A., Sarkar, K., 2011. J. Nanobiotechnol. 9, 1–7.
Choi, O., Hu, Z., 2008. Environ. Sci. Technol. 42, 4583–4588.
Chouhan, R.S., Niazi, J.H., Qureshi, A., 2014. Sens. Actuators B: Chem. 196, 381–387.
de Vasconcelos, E.A., Peres, N.G., Pereira, C.O., da Silva, V.L., da Silva Jr., E.F., Dutra, R. F., 2009. Biosens. Bioelectron. 25, 870–876.
Dickson, J.S., Koohmaraie, M., 1989. Appl. Environ. Microbiol. 55, 832–836.
Hodgson, C., Pethig, R., 1998. Clin. Chem. 44, 2049.
Hussain, S.M., Hess, K.L., Gearhart, J.M., Geiss, K.T., Schlager, J.J., 2005. Toxicol. in vitro 19, 975–983.
Magnusson, K.E., Davies, J., Grundstrom, T., Kihlstrom, E., Normark, S., 1980. Scand. J. Infect. Dis. Suppl. 24, 135–140.
Mcquillan, J.S., Shaw, A.M., 2014. Biosens. Bioelectron. 51, 274–279.
Morones, J.R., Elechiguerra, J.L., Camacho, A., Holt, K., Kouri, J.B., Ramirez, J.T., Yacaman, M.J., 2005. Nanotechnology 16, 2346–2353.
Narayanan, N., Chou, C.P., 2008. Biotechnol. Prog. 24, 293–301.
Nel, A., Xia, T., Madler, L., Li, N., 2006. Science 311, 622–627.
Nel, A.E., Madler, L., Velegol, D., Xia, T., Hoek, E.M.V., Somasundaran, P., Klaessig, F., Castranova, V., Thompson, M., 2009. Nat. Mater. 8, 543–557.
Oberdorster, G., Oberdorster, E., Oberdorster, J., 2005. Environ. Health Perspect. 113, 823–839.
Pompa, P.P., Vecchio, G., Galeone, A., Brunetti, V., Maiorano, G., Sabella, S., Cingolani, R., 2011. Nanoscale 3, 2889–2897.
Qureshi, A., Gurbuz, Y., Kallempudi, S., Niazi, J.H., 2010. Phys. Chem. Chem. Phys. 12, 9176–9182.
Raffa, R.G., Raivio, T.L., 2002. Mol. Microbiol. 45, 1599–1611.
Ribeiro, C., Brogueira, P., Lavareda, G., Carvalho, C.N., Amaral, A., Santos, L., Morgado, J., Scherf, U., Bonifacio, V.D.B., 2010. Biosens. Bioelectron. 26, 1662–1665.
Seetharam, R.N., Sridhar, K.R., 2007. Curr. Sci. 93, 769–770.
Xie, Y.P., He, Y.P., Irwin, P.L., Jin, T., Shi, X.M., 2011. Appl. Environ. Microbiol. 77, 2325–2331.
Zhang, W., Hughes, J., Chen, Y.S., 2012. Appl. Environ. Microbiol. 78, 3905–3915.
Zhang, W., Rittmann, B., Chen, Y.S., 2011. Environ. Sci. Technol. 45, 2172–2178.